Intrinsic dipolar glass behavior in epitaxial films of relaxor $PbMg_{1/3}Nb_{2/3}O_3$

M. Tyunina, M. Plekh, and J. Levoska
Microelectronics and Materials Physics Laboratories, University of Oulu, PL 4500, FI-90014 Oulun yliopisto, Finland
(Received 6 November 2008; revised manuscript received 23 December 2008; published 6 February 2009)

Epitaxial perovskite $PbMg_{1/3}Nb_{2/3}O_3$ films with different thickness (25–750 nm) and relaxed crystal structure are grown on $La_{0.5}Sr_{0.5}CoO_3/MgO$. The intrinsic low-frequency dielectric properties of the films are studied using experimentally determined frequency dispersion of temperature of dielectric maxima, temperature evolution of inverse permittivity and its derivative ξ, and width of dielectric peaks. The intrinsic dipolar glass behavior of the films is evidenced in the temperature range of 80–650 K. The observed thickness dependence of intrinsic properties results from changes in dipolar contribution. Analysis of derivative ξ shows that the low-temperature behavior of the films differs from that of the crystal. The difference is explained by the suppression of the local structural transition in films.

DOI: 10.1103/PhysRevB.79.054105 PACS number(s): 77.84.Dy, 68.65.−k, 77.22.−d, 77.90.+k

I. INTRODUCTION

Perovskite $PbMg_{1/3}Nb_{2/3}O_3$ (PMN) is the best studied relaxor ferroelectric (RFE). The continuous research interest to RFEs (see reviews in Ref. 1) is sustained due to their exceptionally high value of the dielectric constant and the giant piezoelectric effect important for numerous device applications. These unique properties of RFEs are believed to originate from polar nanoregions (or polar clusters) formed at high temperatures and immersed in a matrix. The clusters are considered to be responsible also for the key feature of RFEs: the broad temperature and frequency-dependent maximum of the dielectric permittivity. Although the progress in research methods[2–4] makes it possible to study atomistic mechanisms of cluster behavior, the link between these mechanisms and macroscopic RFE properties is a subject of ongoing discussion.[5,6]

Compared to bulk ceramic or single-crystal RFEs, understanding the properties of RFE thin films is an especially challenging task. In thin films of normal perovskite ferroelectrics (FEs), the presence of lattice strain, film-substrate clamping, electrodes, and small thickness itself result in phase diagrams and dielectric properties essentially different from those of the bulk prototypes.[7] In contrast to extensive phenomenological and first-principles modeling of thin-film FEs, the modeling of thin-film RFEs is at its beginning.[8] The experimental methods applied for studies of clusters in bulk RFE (such as neutron scattering and nuclear magnetic resonance) are not suitable for the films due to the very small amount of film material. The measurements of the dielectric response of thin-film RFEs are affected by the capacitor design or restricted by the substrate material. Also additional difficulties arise due to the technology-related scattering of the properties.

The present work deals with experimental study and analysis of the low-frequency intrinsic dielectric properties of epitaxial PMN films with different thickness. The grown films with a relaxed pseudocubic perovskite structure allow studying the size effect on RFE behavior.

II. EXPERIMENT

Heterostructures of PMN thin films were grown by *in situ* pulsed-laser deposition[9] on MgO(001) single-crystal substrates using an oxide $La_{0.5}Sr_{0.5}CoO_3$ (LSCO) bottom electrode layer. To provide epitaxial growth of pure perovskite PMN, the temperature of deposition 923 K was employed.[9] In the heterostructures, thickness d of PMN films was varied in the range of 25–750 nm, with LSCO thickness kept equal to (150 ± 10) nm.

The crystal structure of the films was analyzed using x-ray diffraction technique as described before.[10] Surface morphology, elemental composition, and thickness of the layers were examined using scanning electron microscopy.[11]

The dielectric response of the capacitor heterostructures with pulsed-laser-deposited Pt top electrodes was measured using a Hewlett-Packard (HP) 4284A *LCR* meter and Linkam LTSE350 MultiProbe stage. The measurements were performed in the out-of-plane direction (normal to substrate surface).

III. RESULTS AND DISCUSSION

A. Crystal structure

The room-temperature Θ-2Θ scans reveal that PMN films are pure perovskite, with a pseudocubic crystal structure oriented with (001) planes parallel to the substrate (001) surface [Fig. 1(a)]. The in-plane (parallel to substrate surface) epitaxial relationship is PMN[100]‖LSCO[100]‖MgO[100].[9,10] In LSCO and PMN films, the out-of-plane lattice parameters c are determined from the Θ-2Θ scans of (004) reflections and the in-plane parameters a from the combination of (004) reflection and the nonspecular (024) reflection. The positions of (024) maxima of PMN are detected at the same φ angle as those of LSCO and MgO, confirming the cube-on-cube epitaxial growth.

The in-plane parameter of LSCO is $a_{LSCO} = 3.864 \pm 0.001$ Å and that of PMN is $a = 4.042 - 4.054$ Å [Fig. 1(b)]. Respectively, the PMN/LSCO lattice mismatch $(a_{LSCO}/a - 1)$ is in the range of $-(4.4\% - 4.9\%)$. In epitaxial heterostructures with a large mismatch, a thin pseudomorphic-strained region near the bottom electrode and a relaxed region (main volume of PMN film) are formed, with a net of misfit dislocations between them. In the x-ray diffraction studies, the main contribution comes from the re-

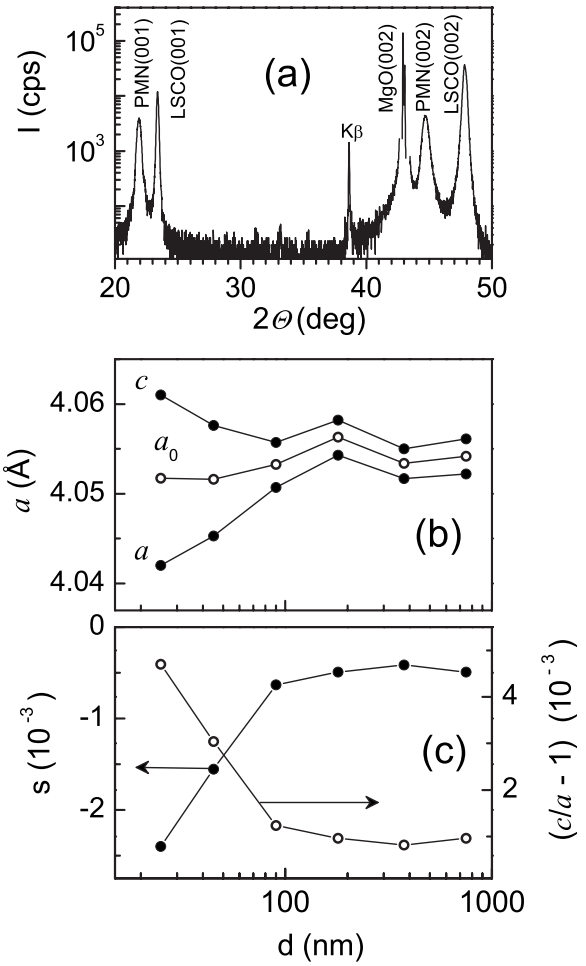

FIG. 1. The crystal structure of PMN films. (a) A typical Θ-2Θ diffraction pattern of PMN/LSCO/MgO heterostructure (thickness of PMN film $d=175$ nm). (b) The in-plane lattice parameter a, out-of-plane lattice parameter c, and average cubic lattice parameter a_0 determined in PMN films as a function of thickness d. (c) The in-plane strain s and out-of-plane tetragonality $(c/a-1)$ as a function of thickness d.

laxed part of the PMN layer. Due to large PMN/LSCO lattice mismatch, the near-electrode-strained layer contains several PMN monolayers only.

In the PMN films, the average strain-free cubic parameter a_0 is calculated using elastic constants for PMN and the measured lattice parameters.[9] The in-plane biaxial strain s in the main part of the film is estimated from the measured in-plane parameter a and the average parameter a_0 using $s=(a/a_0-1)$. The tetragonality of the film is characterized using $(c/a-1)$. With decreasing thickness d, the PMN structure evolves from the fully relaxed pseudocubic to the weakly strained tetragonally distorted one [Fig. 1(c)]. However, even for the thinnest films with $d=25-45$ nm, the magnitude of in-plane compressive strain is very small [Fig. 1(c)] compared to the strain level required for a change in the behavior of thin-film perovskite FEs (Ref. 12) or RFEs.[8] The grown epitaxial PMN films with the relaxed pseudocubic perovskite structure allow us to study mainly the size effect on RFE behavior.

B. Thickness dependence of permittivity

In PMN thin-film heterostructures, the real part of the dielectric permittivity ε and loss factor are determined as a function of temperature T, frequency f, and amplitude E_{ac} of ac electric field using impedance analysis.[13] The impedance Z^* of a leaky thin-film capacitor can be presented as

$$Z^* = R - iX = R_E + \frac{R_F}{1+(\omega C R_F)^2} - i\frac{\omega C R_F^2}{1+(\omega C R_F)^2}, \quad (1)$$

where R_E is the resistance of thin-film electrodes and contacting probes, R_F is the resistance of thin-film PMN, C is the capacitance of heterostructure including thin-film PMN and interfaces, and $\omega=2\pi f$. The resistance term R_F contains Ohmic and dielectric contributions. For $R_F \gg R_E$, the capacitance C is usually found from Eq. (1) using

$$C \approx \frac{X}{\omega(R^2+X^2)}. \quad (2)$$

However, with decreasing thickness of PMN films $d<100$ nm, the resistance R_F becomes dominated by the decreasing Ohmic part. The condition $R_F \gg R_E$ is not satisfied, leading to a profound underestimation of C using Eq. (2). For $d<100$ nm, the capacitance C is extracted from X measured at frequencies $f>100$ kHz using

$$C = \frac{1}{2\omega X}\left(1+\sqrt{1-\frac{4X^2}{R_F^2}}\right), \quad (3)$$

where the dominating Ohmic part of R_F is separately determined using dc measurements of conductance.

In all PMN/LSCO/MgO heterostructures, broad frequency-dependent peaks of $\varepsilon(T)$ are observed [Fig. 2(a)]. The remarkably large maximum permittivity of about 8000 is obtained for $d=750$ nm. With decreasing thickness d from 750 to 45 nm [Fig. 2(b)], the permittivity ε drops by more than 1 order of magnitude in the whole studied range of temperatures. Also the temperature T_{max} decreases [Fig. 2(c)].

In thin-film FE heterostructures, the thickness dependence of the measured ε is commonly described by the interface capacitance model[14] with temperature-independent interface parameters.[15] However, in PMN heterostructures, the dependence of inverse permittivity $1/\varepsilon$ on inverse thickness $1/d$ [Fig. 2(d)] cannot be fitted by an expected linear function at any temperature. For PMN films with similar crystal structure, the results in Fig. 2(d) indicate thickness dependence of intrinsic permittivity ε_{PMN} of PMN films and/or of interface parameters. It should be mentioned that such a thickness dependence can be easily overlooked for FE films with relatively small intrinsic permittivity (several hundreds in FEs compared to tens of thousands in RFEs). It is also obvious that the interface parameters cannot be extracted from $1/\varepsilon \propto 1/d$.

For thin-film RFE heterostructures, the temperature-independent interface contribution can be estimated from the fits $1/\varepsilon=A+B(T-T_A)^2$ at $T>T_{max}$,[16] where the fitting parameter A is determined mainly by the inverse interface capacitance. The static intrinsic permittivity is assumed to be

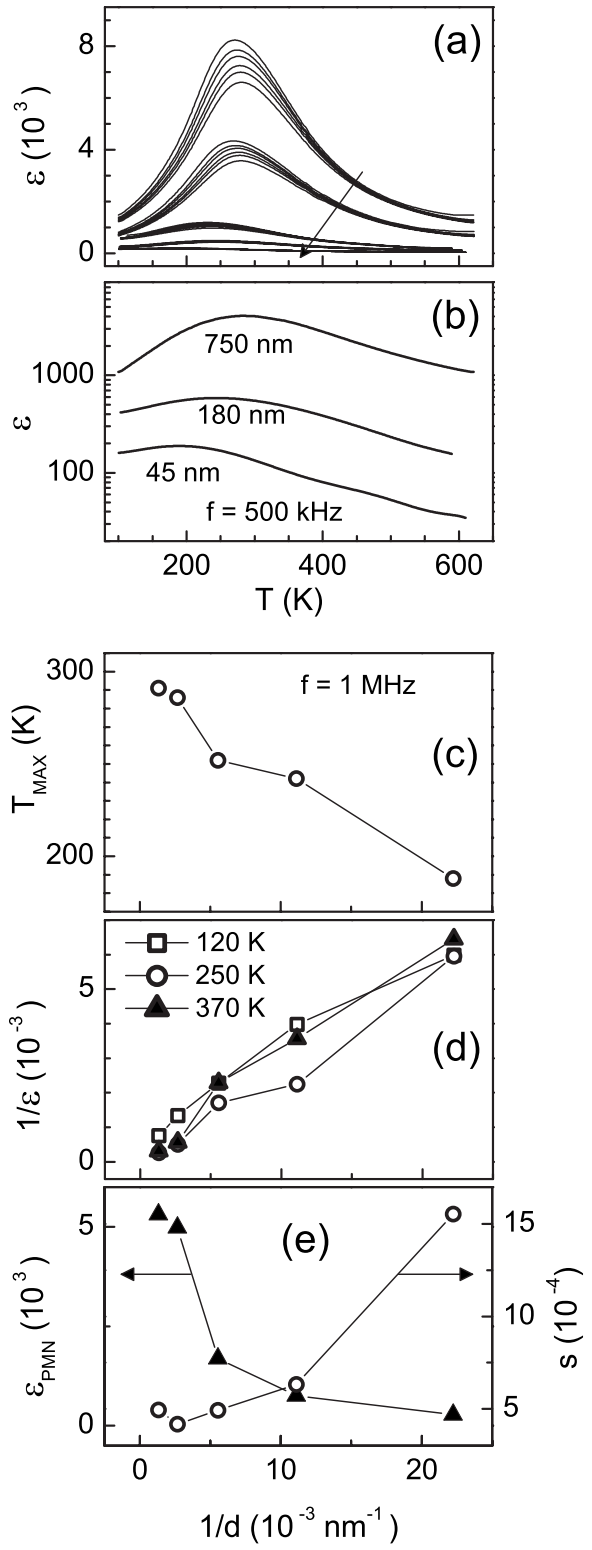

FIG. 2. (a) and (b) The dielectric permittivity ε as a function of temperature T and frequency f determined in PMN/LSCO/MgO heterostructures with different thickness d of PMN films. In (a), frequency $f=1-1000$ kHz and thickness $d=750-45$ nm (as shown by arrow). (c) The temperature of dielectric maximum T_{max}, (d) the measured inverse permittivity $1/\varepsilon$, (e) the reconstructed intrinsic permittivity ε_{PMN}, and the magnitude s of in-plane compressive strain as a function of inverse thickness $1/d$ of PMN films.

considerably larger than $1/A$. Then the intrinsic permittivity ε_{PMN} of PMN films can be reconstructed using ε measured in the heterostructures, parameter A found from the fittings, and an approximate relation $1/\varepsilon_{PMN} \approx 1/\varepsilon - A$. Due to the thickness dependence of T_{max}, the intrinsic permittivity ε_{PMN} in films of different thickness d can be compared only at high temperatures above T_{max}. The reconstructed high-temperature intrinsic permittivity ε_{PMN} is a function of thickness [Fig. 2(e)]. Importantly, the decrease of ε_{PMN} with decreasing d [Fig. 2(e)] correlates with the lowering of T_{max} [Fig. 2(c)]. The drop of ε_{PMN} cannot be related to the in-plane strain; the magnitude of which remains similar for thicknesses of 90–750 nm [Fig. 2(e)].

The results in Fig. 2 show that the intrinsic dielectric permittivity $\varepsilon_{PMN}(f,T)$ of thin-film PMN depends on film thickness.

C. Vogel-Fulcher relationship

The most important characteristic feature of the dielectric behavior of RFEs is the frequency dispersion of permittivity and temperature T_{max}. This is ascribed to the existence of ensemble of relaxators with a broad distribution of relaxation times and temperature evolution of such a system.[5,17] The empirical Vogel-Fulcher relationship between relaxation time and T_{max} is commonly used in the analysis of RFE behavior. In thin-film RFE heterostructures due to the presence of electrodes and interfaces, the relaxation-time spectra cannot be directly found from the measured $\varepsilon(f,T)$. The Vogel-Fulcher relationship between the measurement frequency and T_{max} is analyzed,

$$f = f_0 \exp\left\{-\frac{E_A}{k_B(T_{max} - T_f)}\right\}, \tag{4}$$

where the fitting parameters f_0, E_A, and T_f are related to characteristic relaxation frequency, activation energy, and freezing temperature, respectively. In contrast to the measured value of ε, depending on interface parameters, the temperature T_{max} is not affected by the presence of interface capacitance.

It should be noted that in thin films, also other thermally activated relaxation processes (associated, for instance, with presence of point defects) can principally take place. Generally, they can be described by the Arrhenius-type relationship,

$$f = f_0 \exp\left\{-\frac{E_A}{k_B T_{max}}\right\}. \tag{5}$$

In the studied PMN thin-film heterostructures, the frequency dispersion of T_{max} is analyzed for the films with thickness $d=750-90$ nm, since the low-frequency ($f<100$ kHz) measurements of ε for thinner films are restricted by the low resistance of the films. The Arrhenius-type linear fits to $\ln(f) \propto 1/T_{max}$ can be formally obtained. However, the corresponding fitting parameters are in the ranges of $f_0 \approx 1\times10^{37}-1\times10^{53}$ Hz and $E_A \approx 1.8-2.5$ eV. Such physically unrealistic parameters imply that the relaxation is not of Arrhenius type. The good linear fits to $\ln(f)$

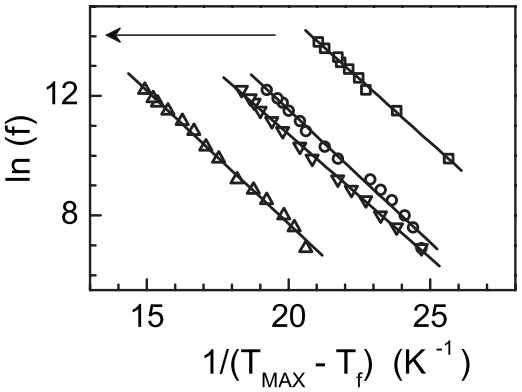

FIG. 3. The relationship between measurement frequency f and temperature of dielectric maximum T_{max}. Solid lines are fits to Vogel-Fulcher relationship $\ln(f) \propto 1/(T_{max}-T_f)$ for the fixed frequency f_0 and arrows show directions of increasing thickness d.

$\propto 1/(T_{max}-T_f)$ suggesting the Vogel-Fulcher-type relaxation are obtained in the studied frequency range of $f = 200$ Hz–1 MHz. The fitting parameters $f_0 \approx 1\times10^{11}-1\times10^{14}$ Hz and $E_A \approx 0.05-0.12$ eV are physically realistic and comparable with those often found in bulk RFEs. In thin-film PMN, the variation of T_f in the interval of ± 15 K around the average value gives fits with approximately similar mean-square deviation. The detected uncertainty in fitting and the spread of T_f are connected to the relatively narrow range of measurement frequencies, which is principally limited by the heterostructure design.[13]

To compare relaxation in different films, the best Vogel-Fulcher fits with similar $f_0 \approx 5\times10^{12}$ Hz are selected [Fig. 3] and the thickness dependences of T_f and E_A are estimated [Fig. 4]. With decreasing thickness, the freezing temperature T_f tends to decrease [Fig. 4(a)] and the activation energy E_A becomes smaller [Fig. 4(b)]. In RFEs, dielectric relaxation is connected mainly with thermally activated flips of polarization of giant dipoles.[1] The tendency in the behavior of E_A can

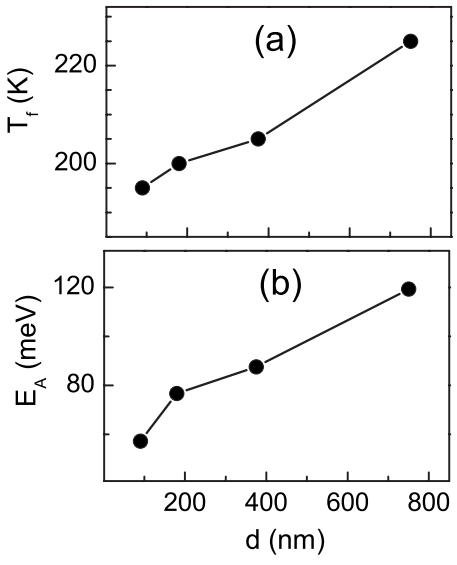

FIG. 4. The Vogel-Fulcher fitting parameters T_f and E_A as a function of thickness d of PMN films for $f_0 = 5\times10^{12}$ Hz.

indicate that the height of barriers between different dipole orientations becomes lower, or the relaxators become "faster" with decreasing d.

In thin-film PMN, the Vogel-Fulcher relationship evidences polarization relaxation typical for RFEs. With decreasing film thickness, such relaxation is found to become faster.

D. High-temperature behavior

In perovskite FEs at high temperatures above the temperature of phase transition, the dielectric permittivity obeys the Curie-Weiss law,

$$\varepsilon = \varepsilon_L + \frac{c}{T-\theta}, \tag{6}$$

where c and θ are the Curie constant and temperature, respectively, and ε_L is about 50.[18] In RFEs at high temperatures above T_{max}, the giant dipoles are known to appear at the Burns temperature $T_B \gg T_{max}$. The Curie-Weiss-type behavior is observed at the temperatures above T_B.

At $T < T_B$, deviation from the high-temperature Curie-Weiss-type behavior is observed. It can be described by the local Edwards-Anderson-type glasslike order parameter. Also, it has been experimentally shown that below T_B, in the 100–200 K wide temperature range above T_{max}, the permittivity follows an empirical scaling law:[19]

$$\frac{\varepsilon_A}{\varepsilon} = 1 + \frac{(T-T_A)^2}{2\delta^2}. \tag{7}$$

Here the fitting parameters ε_A and T_A have been interpreted as the magnitude and temperature of the maximum static permittivity, respectively, and the parameter δ describes high-temperature diffuseness of the dielectric peak.

In thin-film heterostructures due to the presence of interfaces and electrode layers, the intrinsic permittivity of the films cannot be directly assessed from the experimental measurements. The fitting of the measured ε to expressions (6) and (7) does not allow analyzing intrinsic behavior. The temperature evolution of the intrinsic permittivity can be analyzed using the derivative ξ of the measured inverse permittivity $1/\varepsilon$,[20]

$$\xi = \frac{\partial}{\partial T}\left(\frac{1}{\varepsilon}\right), \tag{8}$$

$$\xi = \frac{c}{[\varepsilon_L(T-\theta)+c]^2}, \tag{9}$$

$$\xi = \frac{(T-T_A)}{\delta^2\varepsilon_A}. \tag{10}$$

The expressions (9) and (10) correspond to the Curie-Weiss law (6) and the scaling law (7), respectively.

The behavior of derivative $\xi(f,T)$ is determined by that of intrinsic permittivity $\varepsilon_{PMN}(f,T)$ and possible contributions arising from the temperature dependence of R_E and R_F [see expression (1)]. As seen in Fig. 5, the strong frequency dis-

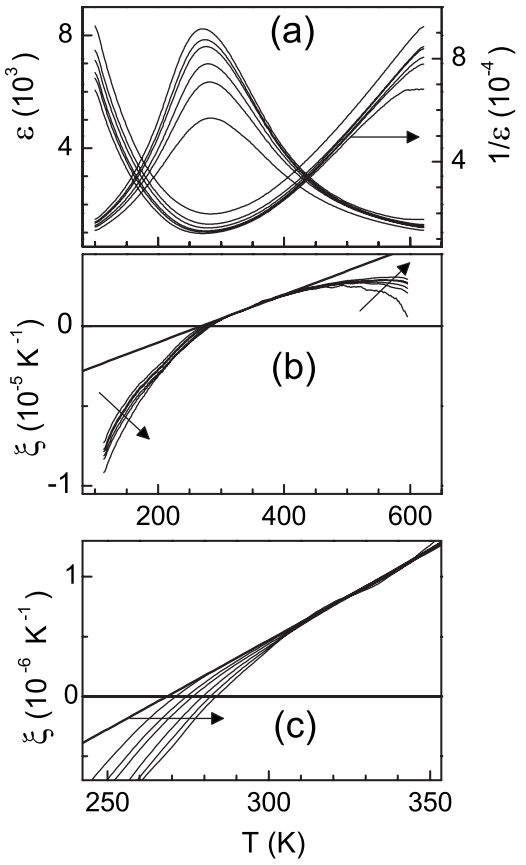

FIG. 5. (a) The measured permittivity ε and inverse permittivity $1/\varepsilon$ and [(b) and (c)] the derivative ξ of inverse permittivity $1/\varepsilon$ as a function of temperature T and frequency in 750 nm thick PMN film. In (b) and (c), straight lines are fits to empirical scaling and arrows show directions of increasing frequency.

persion of the measured ε and $1/\varepsilon$ [Fig. 5(a)] is reduced in $\xi(f,T)$ [Figs. 5(b) and 5(c)]. Above T_{max}, the derivative ξ is frequency independent in a wide temperature range, reflecting intrinsic behavior of ε_{PMN}. The inspection of the measured impedance Z^* shows that the high-temperature frequency dispersion of ξ [at $T>500$ K in Fig. 5(b)] is related to the decrease of R_F (increase in conductance of PMN film). The low-temperature frequency dispersion of ξ [Fig. 5(c)] is equivalent to that of intrinsic ε_{PMN}. Also the good linear fit to $\xi \propto T$ [for 300 K$<T<$400 K in Figs. 5(b) and 5(c)] confirms the intrinsic behavior of $\xi(T)$ consistent with Eqs. (10) and (7). Unfortunately, the high-temperature decrease of R_F makes it difficult to carefully analyze the high-temperature Curie-Weiss-type behavior.

The empirical scaling law is valid above T_{max} [Figs. 6(a) and 6(b)]. The temperature interval of such scaling [Fig. 6(a)] is narrower than that of 200 K in bulk PMN.[19] From the slopes of linear fits to $\xi \propto T$ [Figs. 6(a) and 6(b)], the factor $(\delta^2\varepsilon_A)$ is extracted. In the films with $d=750-375$ nm, this factor is larger than that in single-crystal PMN and it decreases with decreasing thickness d [Fig. 6(c)]. Due to unclear physical mechanism leading to empirical scaling, the analysis of the thickness dependence of $(\delta^2\varepsilon_A)$ is impossible. Importantly, the results in Fig. 6(d) confirm the thickness dependence of intrinsic properties of PMN films.

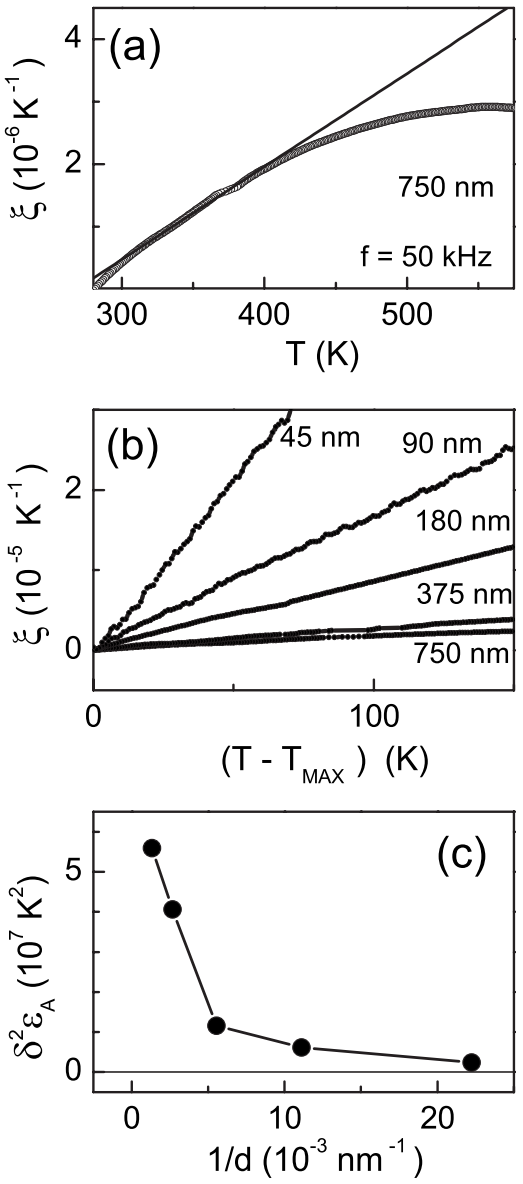

FIG. 6. (a) and (b) The derivative ξ as a function of (a) temperature T or (b) reduced temperature $(T-T_{max})$. In (a) solid line shows fit to empirical scaling. (c) The factor $\delta^2\varepsilon_A$ found from the fits to empirical scaling as a function of inverse thickness $1/d$ of PMN films. The value of $\delta^2\varepsilon_A$ in a PMN crystal is also shown.

In thin-film PMN, the high-temperature dielectric behavior resembles that of bulk PMN. For $d \geq 45$ nm, the empirical scaling is valid above T_{max}.

E. Dipoles and matrix

The dielectric behavior of thin-film PMN is qualitatively similar to that of bulk PMN, as follows from the analysis of the Vogel-Fulcher relationship and the high-temperature behavior. However, a closer inspection of the inverse permittivity $1/\varepsilon$ [Fig. 7(a)] and the derivative ξ [Fig. 7(b)] reveals also a difference between film and bulk. Although smaller permittivity measured in thin-film heterostructures compared to that in bulk PMN can be explained by the presence of

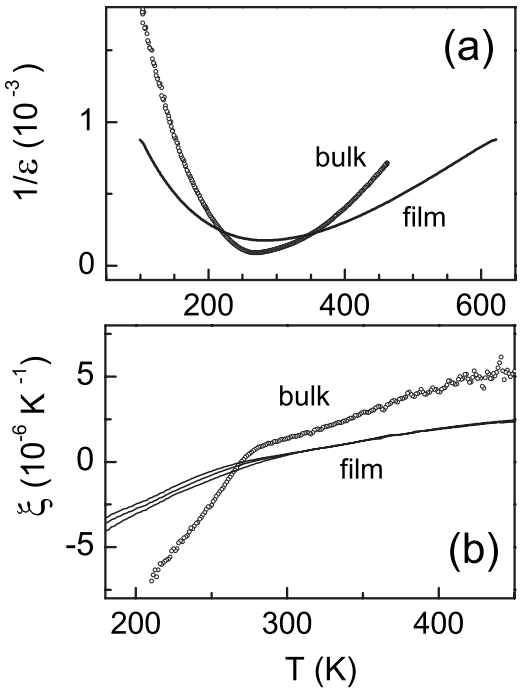

FIG. 7. (a) The inverse permittivity $1/\varepsilon$ and (b) derivative ξ as a function of temperature T determined in 750-nm-thick PMN film (at 100 kHz) and bulk PMN crystal (at 1 MHz).

interface capacitance, the observed profound broadening of the temperature dependence $1/\varepsilon(T)$ [Fig. 7(a)] cannot be ascribed to the interface contribution. Also despite the obtained good fit of $\xi(T)$ to the empirical scaling law at $T>T_{max}$ [Figs. 5(b), 5(c), 6(a), and 6(b)], the shape of $\xi(T)$ in the films differs from that in bulk at the temperatures around and below T_{max} [Fig. 7(b)]. [The derivative $\xi(T)$ for single-crystal PMN is obtained using the results of Ref. 21.] In contrast to the inflection of $\xi(T)$ clearly seen around T_{max} in bulk PMN, such an inflection is smeared in thin films.

In the films in the whole studied range of T, the dependence $\xi(T)$ can be fitted by an empirically found exponential function [Fig. 8(a)],

$$\xi(T) = \xi_0 - \xi_1 \exp\left(-\frac{T}{\xi_2}\right), \tag{11}$$

where ξ_0, ξ_1, and ξ_2 are fitting parameters. As seen from Fig. 8(a), the agreement between the experimentally obtained $\xi(T)$ and the expression (11) is remarkably good. The parameter ξ_0 appears to be practically independent of the measurement frequency. The parameter ξ_1 is larger for higher frequencies, reflecting a steeper drop of $\xi(T)$ on cooling [Fig. 8(a)].

By integrating Eq. (11), an expression for the intrinsic inverse permittivity $1/\varepsilon_{PMN}$ can be obtained,

$$\frac{1}{\varepsilon_{PMN}} = \int \xi(T)dT = \xi_0 T + \xi_1\xi_2 \exp\left(-\frac{T}{\xi_2}\right) + I_{const}, \tag{12}$$

where I_{const} is some integration constant. The measured inverse permittivity $1/\varepsilon$ differs from the intrinsic $1/\varepsilon_{PMN}$ by the interface contribution A (see Sec. III B): $1/\varepsilon = 1/\varepsilon_{PMN} + A$. Using the fitting parameters found from the fit of $\xi(T)$ to Eq. (11) and considering $I_{const}=0$, the temperature-dependent part of Eq. (12) is calculated and compared with the experimentally determined $1/\varepsilon$. A good agreement between the measured and calculated inverse permittivity is found for a certain difference $(I_{const}+A)$ [in Fig. 8(b), the difference is $(I_{const}+A)=-1.2\times10^{-3}$]. Also agreement between the permittivity determined using Eq. (12) and the permittivity measured in the heterostructure is excellent [Fig. 8(c)].

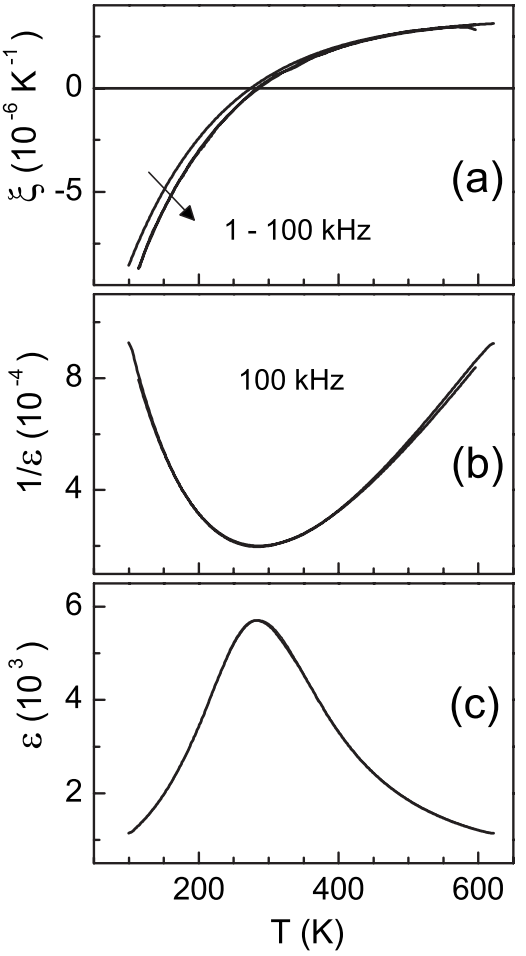

FIG. 8. The (a) derivative ξ, (b) inverse permittivity $1/\varepsilon$, and (c) permittivity ε experimentally determined and obtained by fitting, as a function of temperature in 750-nm-thick PMN film.

The expression (12) can be rewritten in the form,

$$\frac{1}{\varepsilon_{PMN}} = \xi_0\left(T + \frac{I_{const}}{\xi_0}\right) + \xi_1\xi_2 \exp\left(-\frac{T}{\xi_2}\right), \tag{13}$$

where the first term resembles the Curie-Weiss law with the Curie constant $c=1/\xi_0$ and Curie temperature $\theta=-I_{const}/\xi_0$. For the data in Fig. 8(b), the estimated parameters are $c \approx 2.9\times10^5$ K and $\theta \approx 350-380$ K (depending on accuracy of estimation of A). It should be noted that the formally found Curie temperature θ is not related to any phase transition. According to Eqs. (12) and (13), the paraelectriclike state with an apparent Curie-Weiss-type behavior $(1/\varepsilon_{PMN}$

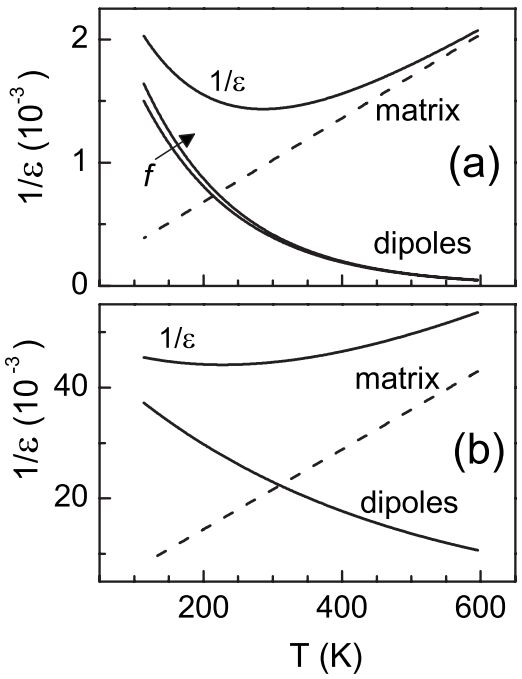

FIG. 9. The temperature-dependent part of the inverse permittivity $1/\varepsilon$ found from the derivative ξ in (a) 750-nm-thick and (b) 90-nm-thick PMN films. The contributions of matrix and dipoles are also shown.

$\propto T$) is asymptotically approached on heating to high-enough temperatures [$T > 550$ K in Fig. 8].

For RFE as an ensemble of giant dipoles embedded in a matrix, the first term of Eq. (12) can be related to such matrix exhibiting paraelectriclike behavior [straight dashed line in Fig. 9(a)]. The second term can describe contribution arising from the thermally activated reorientations of the dipoles [exponential solid lines in Fig. 9(a)]. In the dielectric response of such a two-phase system, the parameters ξ_0 and ξ_1 depend on permittivity and volume fraction of both the matrix and dipoles.[22] The parameter ξ_2 is a measure of dipolar contribution: with increasing ξ_2, the permittivity becomes more dominated by the response of dipoles. On cooling, the role of the dipoles increases [Fig. 9(a)].

In the films with decreasing thickness d from 750 to 45 nm, all fitting parameters ξ_0, ξ_1, and ξ_2 are found to grow. (For instance, the apparent Curie constant drops from about 2.9×10^5 K to 2×10^4 K, by 1 order of magnitude.) The revealed growth of ξ_2 from 135 K to about 400 K corresponds to the relative increase in the dipolar contribution; the temperature dependence of which becomes less steep [Fig. 9(b)]. As seen from Fig. 9, with decreasing d, the lower T_{max}, smaller intrinsic permittivity, and smearing of the intrinsic dielectric peak can be related to the increase of ξ_2, i.e., to the change in dipolar contribution.

In thin-film PMN in the temperature range of 80–650 K, the dielectric response can be interpreted as that of the paraelectriclike matrix with the embedded dipoles. With decreasing thickness, the changes in the dipolar contribution determine the changes in the intrinsic dielectric behavior.

F. Width of dielectric peak

In the PMN films, as seen from expressions (12) and (13) and Fig. 9, the high-temperature dielectric permittivity is determined mainly by that of matrix and the low-temperature permittivity is determined by dipoles. The dielectric peak $\varepsilon(T)$ around T_{max} reflects a transition from the high-temperature law [dominated by the first term in Eq. (12)] to the low-temperature law [dominated by the second term in Eq. (12)]. The temperature interval ΔT around T_{max}, where neither of these laws dominates, can describe the width of the dielectric peak or width of diffuse phase transition in the films.

The width ΔT is limited by the inflection points in $\varepsilon(T)$ at the corresponding characteristic temperatures T_{high} and T_{low}: $\Delta T = T_{high} - T_{low}$. Such width is related to intrinsic thin-film behavior, in contrast to width determined at a certain height of the measured dielectric peak, which depends on heterostructure design.

To study the width of transition, three characteristic temperatures—T_{max}, T_{high}, and T_{low}—are accurately extracted from the measured $\varepsilon(f,T)$ as illustrated in Fig. 10. The temperatures T_{max} are those at which the first derivative is zero: $\varepsilon_{prim} = \partial\varepsilon/\partial T = 0$ [Fig. 10(b)], and the temperatures T_{high} and T_{low} are those at which the second derivative is zero: $\varepsilon_{sec} = \partial^2\varepsilon/\partial T^2 = 0$ [Fig. 10(c)]. The width of transition can be separately analyzed on each side of T_{max} using the low-temperature width $\Delta T_{low} = T_{max} - T_{low}$ and the high-temperature width $\Delta T_{high} = T_{high} - T_{max}$.

In the PMN films, the detected characteristic temperatures depend on frequency [Figs. 11(a)–11(c)]. In contrast to paraelectric-ferroelectric transition in FEs, the diffuse phase transition involves a contribution of dipoles, which exist at $T \gg T_{high}$. The observed temperature $T_{high} \ll T_B$ and frequency dispersion of characteristic temperatures agree with the presence of such dipoles. The existence of the freezing temperature T_f does not mean freezing of motion of all dipoles that explains frequency dispersion of $T_{low} < T_f$. The observed profound increase of T_{low} and weaker increase of T_{high} with increasing frequency agree with the intrinsic behavior illustrated in Fig. 9(a).

With decreasing thickness d of the films, the widths detected at lower frequencies tend to grow, while those determined at higher frequencies remain unchanged or weakly decrease [Fig. 12]. Such controversial tendencies are caused by the presence of dipoles. In thin-film FEs, the broadening of the dielectric peaks with decreasing thickness has been ascribed to the action of internal electric field.[23] A similar mechanism could principally be applied to the static response of RFE film.[8] However, due to the dynamic character of dipolar response, the mechanism of the peak broadening becomes more complicated. The possible internal electric field can affect relaxation-time spectrum, its temperature dependence, and dipolar kinetics.

To illustrate the determining role of the dipolar dynamics in the broadening of the dielectric peaks, the widths ΔT, ΔT_{low}, and ΔT_{high} are analyzed as a function of amplitude E_{ac} of the alternating electric field. According to our previous study,[24] the relaxation-time spectra of thin-film PMN become narrower and shift toward shorter relaxation times with in-

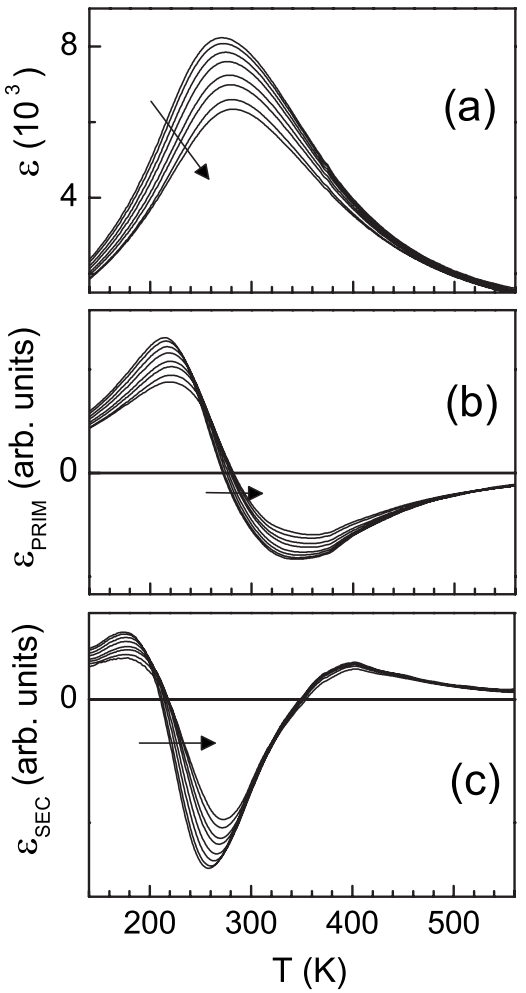

FIG. 10. (a) The measured permittivity ε, (b) first derivative $\varepsilon_{\text{prim}}$, and (c) second derivative ε_{sec} of permittivity as a function of temperature T in 750-nm-thick PMN film (arrows show direction of frequency increase 1–100 kHz).

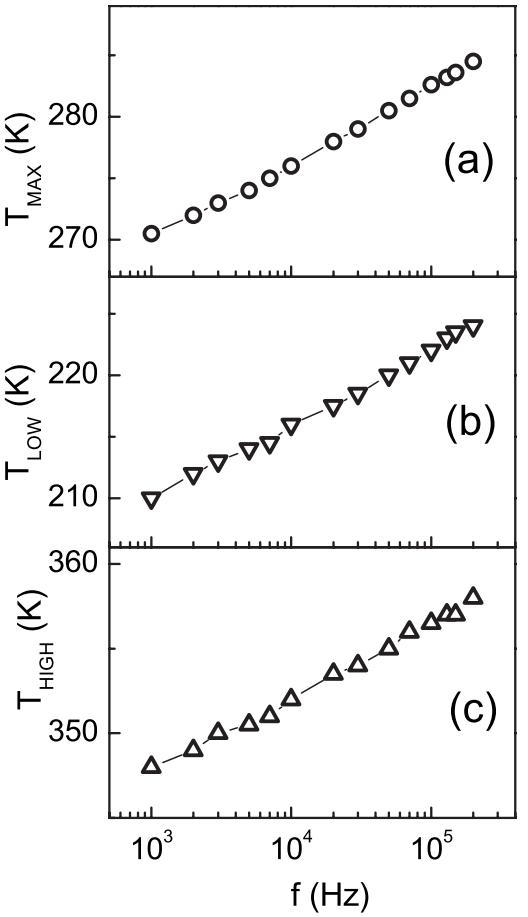

FIG. 11. The characteristic temperatures (a) T_{max}, (b) T_{low}, and (c) T_{high} as a function of frequency f in 750-nm-thick PMN film.

creasing E_{ac}. This can be compared with the tendency to faster relaxation in thinner films found in the present work [Fig. 4]. As seen from Fig. 13, with increasing E_{ac}, the total width ΔT of the dielectric peak becomes larger mainly due to the low-temperature broadening, while the high-temperature width remains less affected. Considering dominant dipolar contribution to the permittivity at low $T<T_{\text{max}}$ [Fig. 9(a)], the results in Fig. 13(c) evidence the major influence of dipoles on the broadening of the dielectric peaks in thin-film PMN.

G. Films versus bulk: dipolar glass and relaxor

The epitaxial PMN films exhibit typical RFE properties, resembling those of bulk PMN. Among these properties are (a) broad frequency-dependent dielectric peaks, (b) frequency dispersion of T_{max} obeying the Vogel-Fulcher relationship, and (c) empirical scaling of the permittivity at high temperatures in the vicinity of T_{max}

Along with these similarities, also the following thickness effects are found. With decreasing thickness, (a) the temperature T_{max} decreases, (b) the freezing temperature T_f decreases and relaxation becomes faster, and (c) scaling factor $\delta^2\varepsilon_A$ decreases and the temperature interval—where the scaling is valid—becomes narrower. There are no models able to explain the observed thickness effects.

Moreover, also features of thin-film behavior, which are in contrast to bulk behavior, are detected. Around T_{max}, the inflection of $\xi(T)$ is found in the PMN crystal. In the films, the inflection is smeared. In the studied range of temperatures 80–650 K, the dielectric response of the films can be presented as that of a paraelectriclike matrix with dipoles, as follows from the excellent exponential fit to $\xi(T)$. In an attempt to understand the observed difference between the films and the crystal, an exponential fitting to $\xi(T)$ of the crystal is tested too.

Such a fitting requires two exponential functions (Fig. 14, instead of one in Fig. 8), which merge at high $T>500$ K. (More details on the fitting will be published elsewhere.) Both the high-temperature fit ξ_{high} ($T>400$ K) and the low-temperature fit ξ_{low} ($T<280$ K) are similar to expression (11) for dipolar glass. The fitting parameters ξ_0 and ξ_2 remain unchanged for ξ_{high} and ξ_{low}, while the parameter ξ_1 drops from the high-temperature value $\xi_1 \approx 8\times10^{-4}$ to the low-temperature value $\xi_1 \approx 3\times10^{-4}$. In the temperature interval $280<T<400$ K, the linear behavior $\xi(T)\propto T$ corresponds to the empirical scaling [expression (10)].

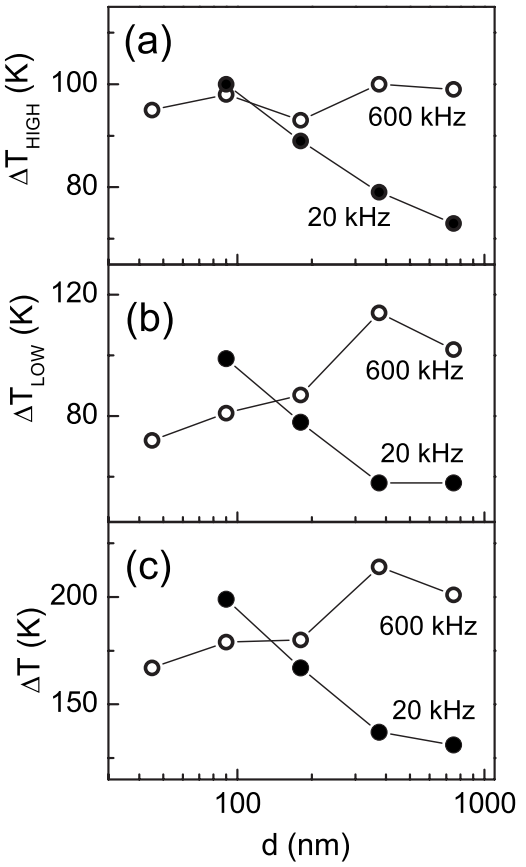

FIG. 12. (a) The high-temperature width ΔT_{high}, (b) low-temperature width ΔT_{low}, and (c) total width ΔT of the dielectric peaks as a function of thickness d of PMN films determined at frequency of 20 and 600 kHz.

Assuming that $\xi(T)$ of the crystal includes contributions from matrix and dipoles, the transformation around T_{max} from ξ_{high} to ξ_{low} by changing ξ_1 can be interpreted as reduction in the volume fraction of the high-temperature dipoles due to the possible appearance of another type of low-temperature dipoles. Remarkably, this interpretation perfectly agrees with the onset of local off-center displacement of Pb and local rhombohedral distortion observed in bulk PMN around and below 300 K.[2,25] Appearance of the low-temperature FE-like dipoles with local rhombohedral structure "draws" ξ_{high} to ξ_{low}. It should be mentioned that using another terminology, the high-temperature ξ_{high} and the FE-like dipoles correspond to "dipolar glass matrix" and "polar nanoclusters," respectively.[3] A two-component system including such "dipolar glass matrix" and "polar nanoclusters" is, actually, a three-component system including paraelectriclike matrix, dipoles, and FE-like dipoles (or polar nanoclusters). At $T<350$ K, the presence of the FE-like dipoles results in the appearance of the longer-time maxima in the distribution of relaxation times.

In contrast to the PMN crystal, there is no detectable difference between ξ_{high} and ξ_{low} in the epitaxial PMN films and the FE-like dipoles are, probably, absent. Importantly, in bulk PMN, the FE-like dipoles are slow.[3] In the films, the revealed fast relaxation (see Sec. III C) agrees with the absence of such slow FE-like dipoles too.

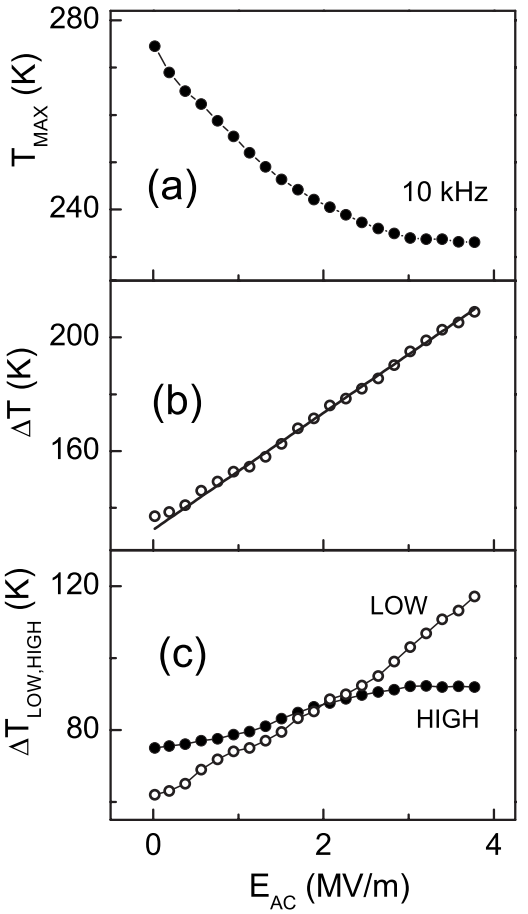

FIG. 13. (a) The temperature T_{max} of dielectric maximum, (b) total width ΔT, (c) high-temperature width ΔT_{high}, and low-temperature width ΔT_{low} of the dielectric peaks as a function of amplitude E_{ac} of ac electric field determined in 750-nm-thick PMN film at $f=10$ kHz.

The apparent absence of the FE-like dipoles might be connected to the suppression of the local structural transition. In epitaxial films of normal perovskite FEs, film-substrate clamping leads to a change or suppression of bulk structural phase transitions.[12] Assuming that also a local structural transition can be influenced by film-substrate clamping, it is easy

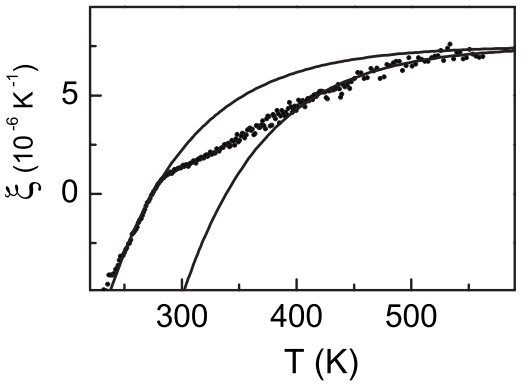

FIG. 14. The derivative ξ as a function of temperature T determined in a PMN crystal at frequency $f=1$ MHz. The exponential fittings are shown by solid lines.

to understand the absence of FE-like dipoles in epitaxial PMN films with relaxed crystal structure [see Fig. 1]. It should be noted that—on the contrary—in strongly strained epitaxial PMN films, due to possible strain-induced local structural transition, the presence of FE-like dipoles might be enhanced.

In the studied PMN films, the observed thickness dependence of the dielectric behavior is related mainly to the change in dipolar contribution evidenced by the increase of $\xi_2 \approx 135-400$ K, exceeding that $\xi_2 \approx 70-85$ K in the crystal. Considering analogous chemical composition and cubic perovskite structure, also similar high-temperature dipoles are expected in films and bulk. The dipolar kinetics (growth of volume fraction of dipoles on cooling), however, can differ, e.g., due to different degrees of disorder.[26] The previously proposed thickness-dependent distribution of random field[27] supports such qualitative explanation.

The results of the present work show that the dielectric properties of epitaxial PMN films are determined by dipoles embedded in a paraelectriclike matrix (dipolar glass). The FE-like dipoles or polar nanoclusters, which are responsible for the low-temperature relaxor behavior in bulk PMN, are absent in the films. Nevertheless, the main RFE features of bulk PMN (with FE-like dipoles) are still preserved in thin-film PMN (without FE-like dipoles).

From the performed comparison of thin film and bulk behavior, it seems that the main RFE characteristics of bulk PMN (broad frequency-dependent dielectric peak, Vogel-Fulcher relationship, and deviation from the high-temperature Curie-Weiss-type behavior) result mainly from the dipoles (ξ_{high}). The FE-like dipoles or polar clusters create only additional low-temperature contribution to the dielectric response. The hypothesis requires further investigations.

IV. CONCLUSIONS

Epitaxial perovskite PMN films with different thickness (25–750 nm) and relaxed crystal structure are grown on LSCO/MgO. The dielectric response of the Pt/PMN/LSCO/MgO capacitor heterostructures is measured as a function of temperature, frequency, and electric field. The intrinsic dielectric properties of the PMN films are studied using the detailed analysis of the frequency dispersion of T_{max}, of the temperature evolution of inverse permittivity $1/\varepsilon$ and its derivative ξ, and of the width of dielectric peaks.

The intrinsic properties of the films resemble those of bulk PMN. With decreasing thickness, the temperatures T_{max} and T_f, the relaxation time, the scaling factor $\delta^2\varepsilon_A$, and the temperature interval of scaling decrease and the widths of the peaks change. The excellent exponential fit to $\xi(T)$ is obtained in the temperature range of 80–650 K, suggesting contributions from a paraelectriclike matrix and dipoles. The observations evidence dipolar glass behavior. The thickness dependence of intrinsic properties results from changes in the dipolar contribution.

The low-temperature dielectric behavior of the films differs from that of bulk PMN, where an additional contribution from the FE-like dipoles is detected below 350 K and ascribed to the local structural transition. The difference is explained by the suppression of the local structural transition due to film-substrate clamping.

ACKNOWLEDGMENTS

The authors of Ref. 21 are acknowledged for their kind permission to use some of their experimental results. The work is supported by the Academy of Finland (under Grant No. 118250) and by Infotech Oulu Graduate School (M.P.).

[1] For reviews, see A. A. Bokov and Z.-G. Ye, J. Mater. Sci. **41**, 31 (2006); G. A. Samara, J. Phys.: Condens. Matter **15**, R367 (2003).
[2] W. Dmowski, S. B. Vakhrushev, I.-K. Jeong, M. P. Hehlen, F. Trouw, and T. Egami, Phys. Rev. Lett. **100**, 137602 (2008).
[3] R. Blinc, V. V. Laguta, B. Zalar, and J. Banys, J. Mater. Sci. **41**, 27 (2006).
[4] I. Grinberg, P. Juhas, P. K. Davies, and A. M. Rappe, Phys. Rev. Lett. **99**, 267603 (2007).
[5] R. Pirc and R. Blinc, Phys. Rev. B **76**, 020101(R) (2007).
[6] R. Pirc and R. Blinc, Phys. Rev. B **60**, 13470 (1999); R. Pirc, R. Blinc, and V. Bobnar, *ibid.* **63**, 054203 (2001); B. E. Vugmeister, *ibid.* **73**, 174117 (2006); D. Viehland, J. F. Li, S. J. Jang, L. E. Cross, and M. Wuttig, *ibid.* **43**, 8316 (1991); M. D. Glinchuk and R. Farhi, J. Phys.: Condens. Matter **8**, 6985 (1996); B. E. Vugmeister and M. D. Glinchuk, Rev. Mod. Phys. **62**, 993 (1990); A. Bussmann-Holder, A. R. Bishop, and T. Egami, Europhys. Lett. **71**, 249 (2005); J. Hlinka, S. Kamba, J. Petzelt, J. Kulda, C. A. Randall, and S. J. Zhang, Phys. Rev. Lett. **91**, 107602 (2003).
[7] M. Dawber, J. F. Scott, and K. M. Rabe, Rev. Mod. Phys. **77**, 1083 (2005); N. Setter, D. Damjanovic, L. Eng, G. Fox, S. Gevorgian, S. Hong, A. Kingon, H. Kohlstedt, N. Y. Park, G. B. Stephenson, I. Stolitchnov, A. K. Taganstev, D. V. Taylor, T. Yamada, and S. Streiffer, J. Appl. Phys. **100**, 051606 (2006).
[8] E. A. Eliseev and M. D. Glinchuk, J. Appl. Phys. **102**, 104110 (2007).
[9] M. Tyunina and J. Levoska, J. Appl. Phys. **97**, 114107 (2005).
[10] J. Levoska, M. Tyunina, A. Sternberg, and S. Leppävuori, Ferroelectrics **271**, 137 (2002); J. Levoska and M. Tyunina, *ibid.* **291**, 11 (2003).
[11] M. Tyunina, J. Levoska, A. Sternberg, and S. Leppävuori, J. Appl. Phys. **86**, 5179 (1999); M. Tyunina, J. Levoska, and S. Leppävuori, *ibid.* **91**, 9277 (2002).
[12] N. A. Pertsev, A. G. Zembilgotov, and A. K. Tagantsev, Phys. Rev. Lett. **80**, 1988 (1998).
[13] M. Tyunina, J. Phys.: Condens. Matter **18**, 5725 (2006).
[14] S. L. Miller, R. D. Nasby, J. R. Schwank, M. S. Rodgers, and P. V. Dressendorfer, J. Appl. Phys. **68**, 6463 (1990).
[15] N. A. Pertsev, R. Dittmann, R. Plonka, and R. Waser, J. Appl. Phys. **101**, 074102 (2007) and references therein.
[16] M. Tyunina and J. Levoska, Phys. Rev. B **72**, 104112 (2005).

[17] M. D. Glinchuk and V. A. Stephanovich, J. Appl. Phys. **85**, 1722 (1999).
[18] G. Rupprecht and R. O. Bell, Phys. Rev. **135**, A748 (1964).
[19] A. A. Bokov, Y.-H. Bing, W. Chen, Z.-G. Ye, S. A. Bogatina, I. P. Raevski, S. I. Raevskaya, and E. V. Sahkar, Phys. Rev. B **68**, 052102 (2003).
[20] M. Tyunina and J. Levoska, Appl. Phys. Lett. **89**, 196102 (2006); M. Tyunina, J. Levoska, and I. Jaakola, Phys. Rev. B **75**, 140102(R) (2007).
[21] V. Bovtun, S. Kamba, A. Pashkin, M. Savinov, P. Samoukhina, J. Petzelt, I. P. Bykov, and M. D. Glinchuk, Ferroelectrics **298**, 23 (2004).
[22] See, e.g., B. Sareni, L. Krahenbuhl, A. Beroual, and C. Brosseau, J. Appl. Phys. **80**, 1688 (1996) and references therein.
[23] M. D. Glinchuk and A. N. Morozovska, J. Phys.: Condens. Matter **16**, 3517 (2004); A. M. Bratkovsky and A. P. Levanyuk, Phys. Rev. Lett. **94**, 107601 (2005).
[24] M. Tyunina and J. Levoska, Phys. Rev. B **72**, 104112 (2005).
[25] T. Egami, E. Mamontov, W. Dmowski, and S. B. Vakhrushev, AIP Conf. Proc. **677**, 48 (2003); I.-K. Jeong, T. W. Darling, J. K. Lee, Th. Proffen, R. H. Heffner, J. S. Park, K. S. Hong, W. Dmowski, and T. Egami, Phys. Rev. Lett. **94**, 147602 (2005).
[26] R. Paul, S. Puri, and H. Rieger, Phys. Rev. E **71**, 061109 (2005).
[27] E. A. Eliseev and M. D. Glinchuk, Ferroelectrics **316**, 167 (2005).